Supporting Information

Guaiacol Hydrogenation in Methanesulfonic Acid Using a Stirred Slurry Electrocatalytic Reactor: Mass Transport and Reaction Kinetics Aspects

Yanuar Philip Wijaya,[a,b] Robertus D. D. Putra,[a,b] Kevin J. Smith,[a,*] Chang Soo Kim,[b,c,*] Elöd L. Gyenge[a,*]

[a]*Department of Chemical and Biological Engineering, The University of British Columbia, 2360 East Mall, Vancouver, BC, V6T 1Z3, Canada*

[b]*Department of Chemical and Biological Engineering, The University of British Columbia, KIST-UBC Biorefinery On-site Laboratory, 2259 Lower Mall, Vancouver, BC, V6T 1Z4, Canada*

[c]*Clean Energy Research Center, Korea Institute of Science and Technology, Seoul 02792, Republic of Korea*

*Corresponding authors. *E-mail addresses*: kjs@mail.ubc.ca (K. J. Smith), mizzou333@kist.re.kr (C. S. Kim), egyenge@chbe.ubc.ca (E. L. Gyenge).

Number of Pages: 31

Number of Figures: 10

Number of Tables: 1

Number of Schemes: 1

Table of Contents

Catalyst characterization

N$_2$ physisorption measurements were performed in a surface area and porosity analyzer (Micromeritics ASAP 2020) at 77 K to determine Brunauer-Emmett-Teller (BET) surface areas and pore volumes of the catalysts, along with the average pore diameter by Barrett-Joyner-Halenda (BJH) method. The sample was degassed at 200 °C for 2 h before measurement. CO chemisorption was performed in Micromeritics AutoChem II equipped with thermal conductivity detector (TCD) using a pulsed injection of 5% CO/He to measure the metal surface area. Prior to measurement, the sample was reduced under H$_2$ flow (50 cm^3/min) at 300 °C for 1 h. The catalyst characterization results are presented in Figure S1 and Table S1.
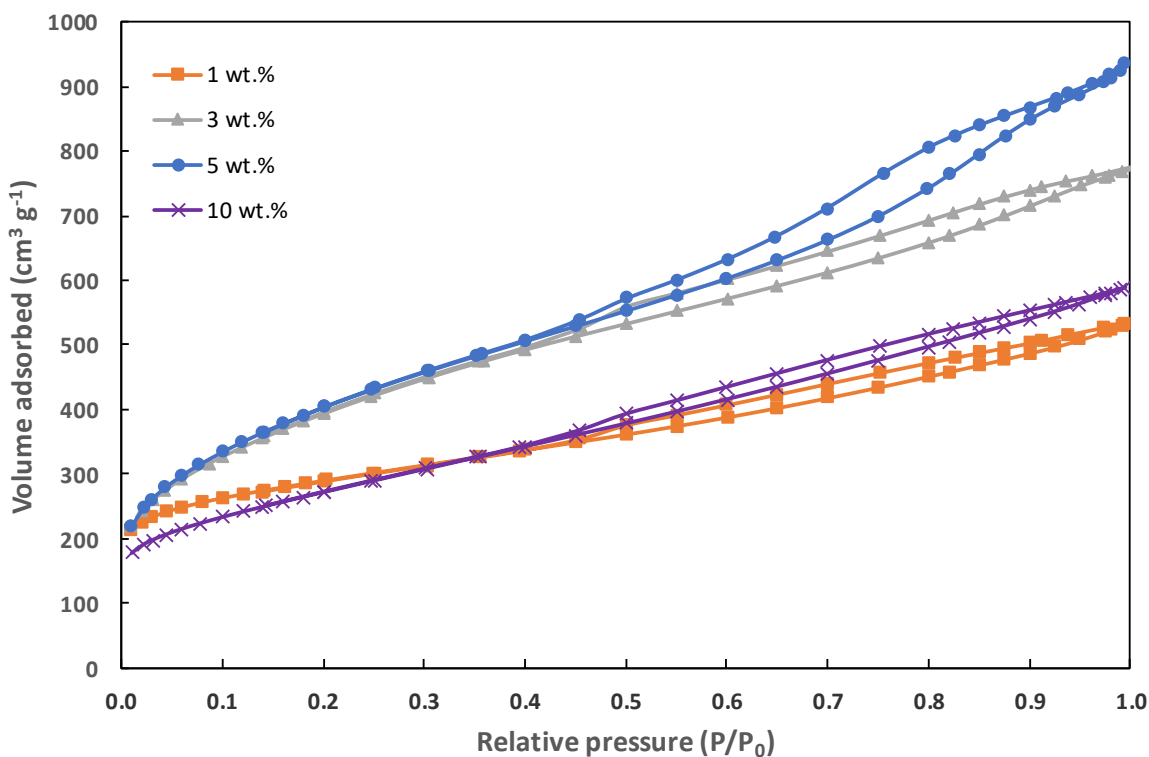

Figure S1. Adsorption-desorption isotherms for Pt/C with different metal contents.

Table S1. Characteristics of the Pt-C catalysts used in this study.

Pt content (wt.%)	S_{BET}[a] (m²/g)	V_{pore}[b] (cm³/g)	D_{pore}[c] (nm)	φ (%)	S_{metal} (m²/g)	d_p (nm)
1	1010	0.82	4.36	36.98	91.32	3.06
3	1448	1.19	3.70	14.55	35.94	7.78
5	1487	1.43	4.35	28.95	71.50	3.91
5*	138	0.29	6.16	18.23	45.04	6.21
10	972	0.91	4.17	8.45	20.87	13.40

[a] BET surface area;

[b] Single point adsorption total pore volume ($P/P_0 = 0.99$);

[c] Average pore diameter by BJH desorption;

φ (metal dispersion), S_{metal} (metallic surface area), and d_p (active particle diameter) determined by CO chemisorption.

*Exception case for Pt/Al_2O_3.

Potentiostatic guaiacol ECH results: Effect of catalyst support

Different catalyst supports (i.e., carbon vs alumina) which possess largely different electrical conductivity were compared in the guaiacol ECH using dilute H_2SO_4 electrolyte (0.2–0.5 M). With the same bulk catalyst amount (0.10 g, R/M = 314), Pt/C showed superior performance than Pt/Al$_2$O$_3$ (Figure S2), resulting in nearly 8 times higher guaiacol conversion and 10 times higher F.E. This could be attributed to the superior current distribution in the catalyst particle bed with the electronically conductive carbon support combined with more favorable structural properties (e.g., surface area, pore volume, and metal dispersion) (Table S1). With Al$_2$O$_3$ support about 8.5 times higher amount than C is required Pt/Al$_2$O$_3$ (0.85 g, R/M = 37) to achieve comparable ECH reactivity (Figure S2a-b). At the higher electrolyte concentration (0.5 M), comparably high guaiacol conversion (92% vs. 96%) and cyclohexanol selectivity (49% vs. 51%) were obtained despite the moderate F.E. (31% vs. 35%) in comparison with the low loading of Pt/C (Figure S2b). In a separate electrolysis experiment using only activated carbon support no hydrogenation products were formed at all showing the importance of dispersed metal sites.[1,2] No stark differences were observed in terms of the product distribution, implying that the different catalyst supports did not influence the reaction pathways under the operating conditions.
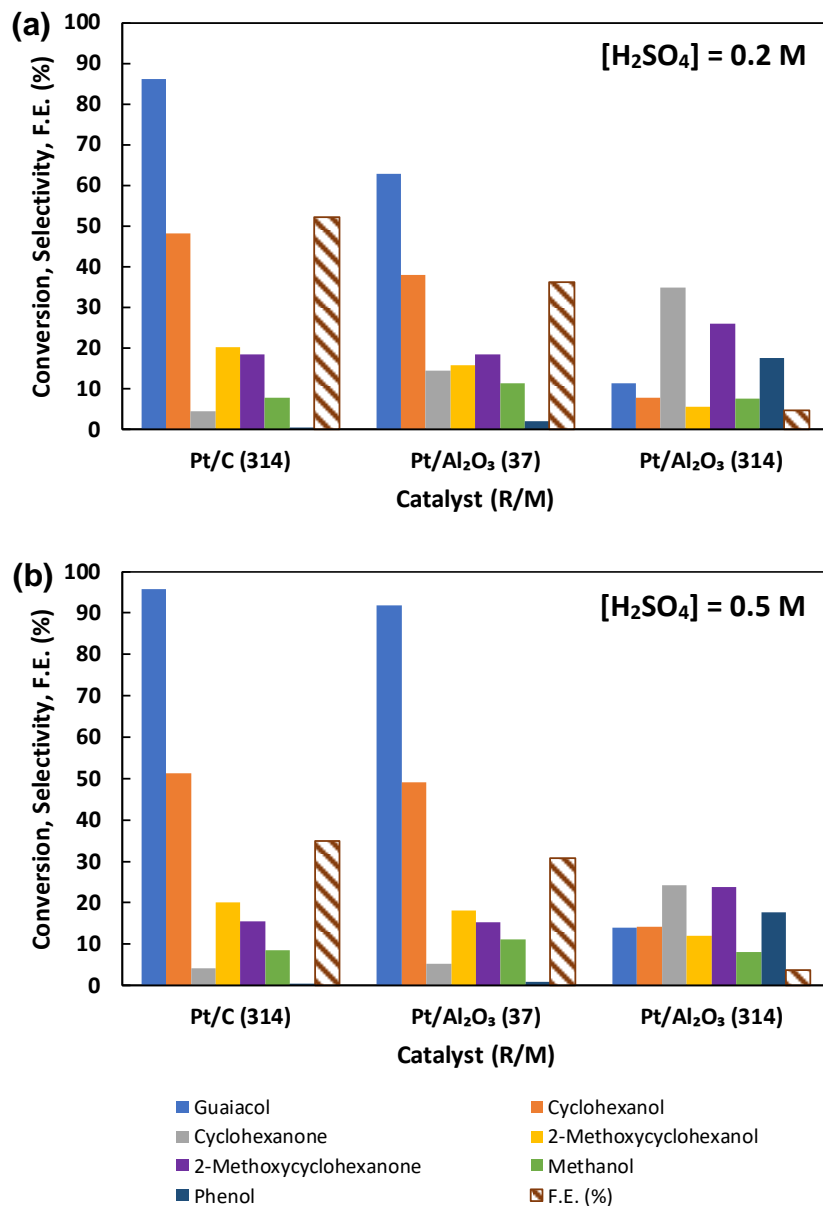
Figure S2. ECH of guaiacol in H_2SO_4 electrolyte: (a) 0.2 M, (b) 0.5 M. Guaiacol conversion, product selectivity, and Faradaic efficiency profiles for different catalyst support materials. Reaction conditions: E = -1.25 V (vs. Ag/AgCl), $T \approx 42$ °C, t = 4 h, R_d = 350 rpm (Stirrer A), (a) $I \approx$ -0.57 A (j = -206 mA cm^{-2}), (b) $I \approx$ -0.95 A (j = -345 mA cm^{-2}). Catalyst: 5 wt.%-Pt/C (0.10 g), 5 wt.%-Pt/Al_2O_3 (0.10 g and 0.85 g). Guaiacol concentration (initial) = 0.1 M. R/M = reactant/metal molar ratio. Molecular weight of the catalyst support: M_w = 12.01 (carbon), 101.96 (alumina).

Mass-transfer limitation assessment in the ECH of guaiacol

Internal mass-transfer resistance (Weisz-Prater criterion)

In heterogeneous catalytic reactions, the Weisz-Prater (W–P) criterion is used to estimate the influence of pore diffusion on reaction rates. If the criterion is satisfied, pore diffusion limitations (internal mass-transfer resistance) is negligible. The W–P criterion[3] is given below:

$$N_{W-P} = \frac{-r_A \rho_p R_p^2}{C_s D_{eff}} \leq \frac{1}{n} \tag{S1}$$

where $-r_A$ = reaction rate per mass of dispersed metal catalyst (mol s^{-1} kg^{-1}), ρ_p = density of catalyst (kg m^{-3}), R_p = catalyst particle radius (m), C_s = reactant concentration at the catalyst surface (mol m^{-3}), D_{eff} = effective diffusivity (m^2 s^{-1}), n = reaction order (1). In a stirred slurry reactor, $C_{A0} \approx C_s$ (the boundary layer thickness is negligible).

Guaiacol ECH experimental data (C_{A0}, $-r_A$), catalyst properties data ($\rho_{p,Pt}$ = 21.45 g cm^{-3}, $d_{p,Pt}$ = 3.91 nm from Table S1) and guaiacol diffusivity data (D_{eff} = 4.22×10^{-8} m^2 s^{-1}, calculated by Knudsen diffusivity: $D_{KA} = \frac{d}{3}\sqrt{\frac{8RT}{\pi M_A}}$, where d = pore diameter = 4.35 nm, R = 8.314 J mol^{-1} K^{-1}, T = 50 °C, M_A = guaiacol molar mass = 124 g mol^{-1}) can be used to estimate N_{W-P} as follows:

C_{A0} (mM)	$-r_A$ (mmol s^{-1} g$_{Pt}^{-1}$)	N_{W-P}	
53	3.41×10^{-1}	1.24×10^{-8}	
80	3.89×10^{-1}	9.46×10^{-9}	$N_{W-P} \ll 1$
106	4.03×10^{-1}	7.38×10^{-9}	
132	4.14×10^{-1}	6.08×10^{-9}	

In all cases, $N_{W-P} \ll 1$, thus internal mass-transfer resistance is negligible. In other words, reaction rates are not affected by guaiacol diffusion rate to the catalyst pore.

External mass-transfer resistance (Sherwood number)

Sherwood number represents the ratio of the convective mass transfer to the rate of diffusion:

$$S_h = \frac{k_{S-L} \, d_p}{D_{eff}}$$
(S2)

The mass-transfer coefficient from liquid to solid (k_{S-L}) is calculated from Sherwood number as follows, with the catalyst geometry is assumed to be spherical:[4]

$$S_h = 2 + 0.4 Re^{1/4} Sc^{1/3}$$
(S3)

Reynolds number (Re) for a stirred vessel can be approximated as:

$$Re = \frac{\rho \, N \, r^2}{\mu}$$
(S4)

Schmidt number (Sc) is the ratio of viscous diffusion rate and mass (molecular) diffusion rate:

$$Sc = \frac{\mu}{\rho D}$$
(S5)

where ρ = density of the solution, μ = viscosity of the solution, N = rotational speed, r = radius of the stirrer, D = mass diffusivity (= D_{eff}), d_p = catalyst particle diameter.

Equations S2–S5 can be solved using the following experimental data: $\rho = 1.01$ g cm^{-3}, $\mu = 5.5 \times 10^{-4}$ Pa. s (at 50 °C), $N = 240$ rpm, $r = 1.8$ cm, resulting in: $Sc = 904$, $Re = 2374$, $Sh = 29$, and $k_{S-L} = 2.34 \times 10^{-4}$ m s^{-1}.

If external mass-transfer resistance is not significant (i.e. surface reaction is very fast), this correlation applies:[5,6]

$$\left(\frac{1}{-r_A} \ll \frac{1}{k_{S-L}\, a_p\, C_{A0}}\right) \text{ or } \left(-r_A \gg k_{S-L}\, a_p\, C_{A0}\right) \tag{S6}$$

where the particle surface area per unit volume is given by: $a_p = \frac{6w}{\rho_p d_p}$ for spherical catalyst ($w =$

catalyst loading per unit volume of liquid phase = 1.5 kg m^{-3}, $\rho_{p,Pt/C} = 2.97$ g cm^{-3}, $d_{p,Pt/C} =$

75 μm), thus $a_p = 40.37$ m^{-1} and Equation S6 can be calculated further to obtain the following:

C_{A0} (mM)	$-r_A$ (mol s^{-1} m^{-3})	$k_{S-L}\, a_p\, C_{A0}$	
53	1015	1.74×10^{-2}	
80	1156	2.60×10^{-2}	$-r_A \gg k_{S-L}\, a_p\, C_{A0}$
106	1198	3.45×10^{-2}	
132	1230	4.30×10^{-2}	

In all cases, $-r_A \gg k_{S-L}\, a_p\, C_{A0}$, thus external mass-transfer resistance is negligible. In other

words, reaction rates are not affected by guaiacol diffusion rate to the catalyst surface.

Overall, this mass-transfer limitation assessment demonstrates that the guaiacol ECH rates are

kinetically controlled under the operating conditions in this study.
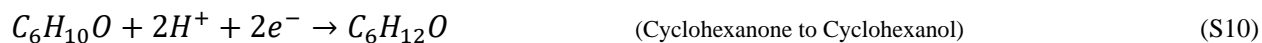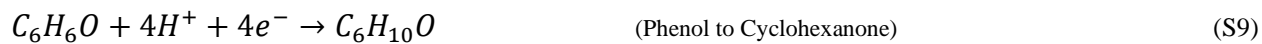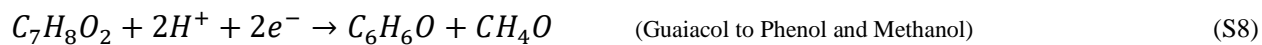
Catalytic reaction steps in ECH of guaiacol
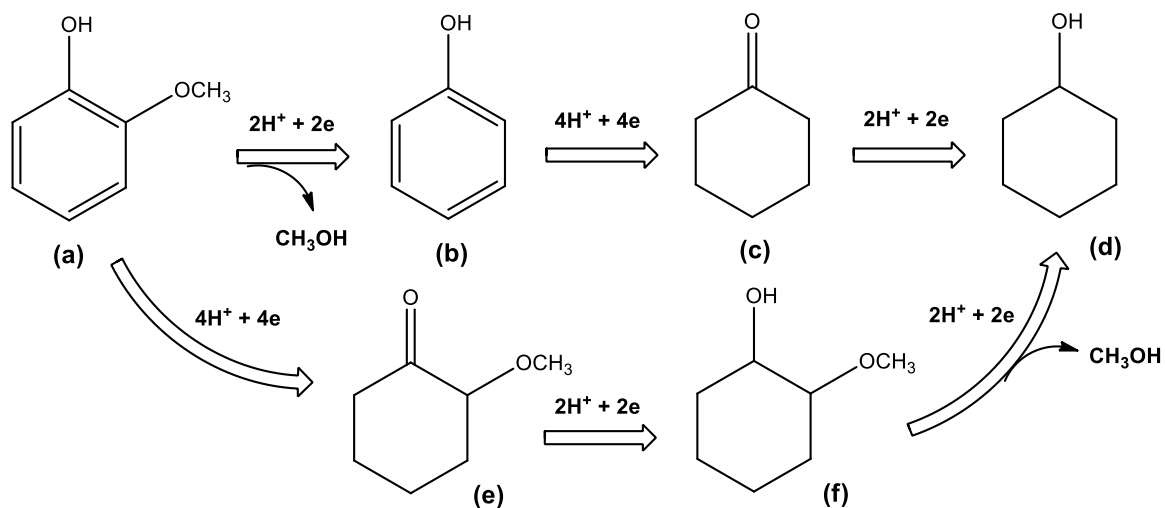
Scheme S1. Plausible reaction network in the ECH of guaiacol under the experimental conditions in this work.

Guaiacol ECH (Overall Reaction):

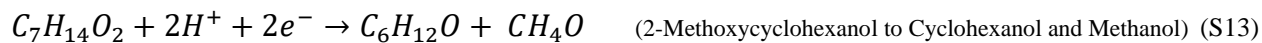$$C_7H_8O_2 + 8H^+ + 8e^- \rightarrow C_6H_{12}O + CH_4O \tag{S7}$$
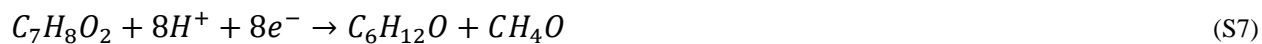
Two Parallel Routes in the Guaiacol ECH:

1. Demethoxylation – Ring Saturation

$$C_7H_8O_2 + 2H^+ + 2e^- \rightarrow C_6H_6O + CH_4O \qquad \text{(Guaiacol to Phenol and Methanol)} \tag{S8}$$

$$C_6H_6O + 4H^+ + 4e^- \rightarrow C_6H_{10}O \qquad \text{(Phenol to Cyclohexanone)} \tag{S9}$$

$$C_6H_{10}O + 2H^+ + 2e^- \rightarrow C_6H_{12}O \qquad \text{(Cyclohexanone to Cyclohexanol)} \tag{S10}$$

2. Ring Saturation – Demethoxylation

$$C_7H_8O_2 + 4H^+ + 4e^- \rightarrow C_7H_{12}O_2 \qquad \text{(Guaiacol to 2-Methoxycyclohexanone)} \tag{S11}$$

$$C_7H_{12}O_2 + 2H^+ + 2e^- \rightarrow C_7H_{14}O_2 \qquad \text{(2-Methoxycyclohexanone to 2-Methoxycyclohexanol)} \tag{S12}$$

$$C_7H_{14}O_2 + 2H^+ + 2e^- \rightarrow C_6H_{12}O + CH_4O \qquad \text{(2-Methoxycyclohexanol to Cyclohexanol and Methanol)} \tag{S13}$$
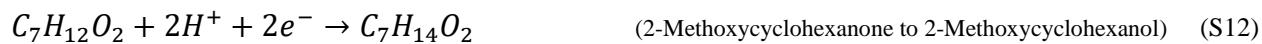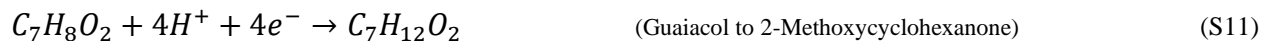
Reaction network and mechanism study in the ECH of guaiacol

Prior to detailed kinetic analysis, the rate-determining step (RDS) in the guaiacol ECH was first determined through comparison between the assumed reaction mechanism and the rate data. In formulating the rate law for guaiacol ECH, the experimental rate data were ensured to be governed by reaction kinetic rather than mass transport. Under the operating conditions, the fluid velocities were large enough at the optimum stirring rates while the catalyst particles were small enough such that neither external diffusion nor internal diffusion is limiting. The RDS was determined based on Langmuir–Hinshelwood mechanism and the derived rate law was then compared with the best fitting experimental data. As in classic heterogeneous catalysis, three possible scenarios were evaluated to verify the RDS: adsorption, surface reaction, or desorption-limited reaction.[7] The mathematical derivations are provided in the following section. There was a linear relationship between the initial reaction rate and the initial guaiacol concentration, either under potentiostatic or galvanostatic conditions (Figure S3), confirming our observation in the previous work.[1] At low guaiacol concentrations, this linear relationship could imply either adsorption at low surface coverage (i.e., Henry's linear isotherm is applicable) or apparent 1st order surface reaction-controlled mechanism.
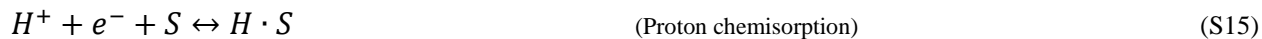
Guaiacol ECH mechanism is hence different than that of phenol ECH, indicating the different reactivity toward hydrogen radicals. Phenol ECH was found to be zero-order reaction implying that the reaction rate is independent of the initial phenol concentration due to surface coverage saturation.[1,8] In contrast to phenol ECH which proceeds in a series reaction to cyclohexanone and cyclohexanol, guaiacol ECH occurs in a parallel pathway involving demethoxylation and aromatic ring saturation steps (Scheme S1).

Formulating the rate law and verifying the rate-determining step

This approach is based on Langmuir–Hinshelwood kinetic mechanism.[7] All the elementary steps are assumed as first-order, reversible, dual-site reaction with competitive adsorption and uniform surface activity. The organic reactants are adsorbed on the catalyst surface through molecular or non-dissociative adsorption.
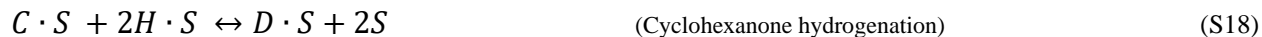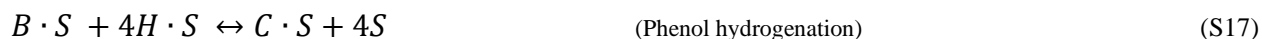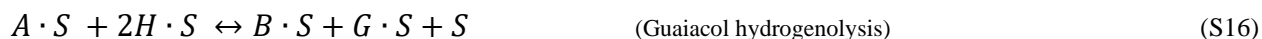
The organic compounds in Scheme S1 are denoted as follows: Guaiacol (A), Phenol (B), Cyclohexanone (C), Cyclohexanone (D), 2-Methoxycyclohexanone (E), 2-Methoxycyclohexanol (F), and Methanol (G).

All the elementary steps involved in the ECH of guaiacol can then be written as follows (with S denoting the catalyst surface active sites):

$$A + S \leftrightarrow A \cdot S \qquad \text{(Guaiacol adsorption)} \qquad \text{(S14)}$$

$$H^+ + e^- + S \leftrightarrow H \cdot S \qquad \text{(Proton chemisorption)} \qquad \text{(S15)}$$
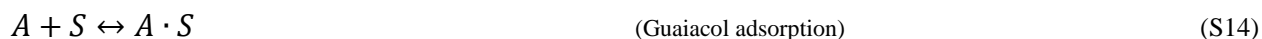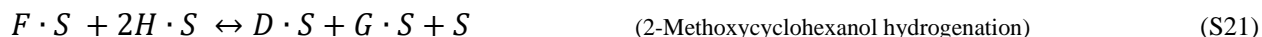
The surface reaction is derived from the following elementary steps:

Route 1: Demethoxylation – Ring Saturation

$$A \cdot S + 2H \cdot S \leftrightarrow B \cdot S + G \cdot S + S \qquad \text{(Guaiacol hydrogenolysis)} \qquad \text{(S16)}$$

$$B \cdot S + 4H \cdot S \leftrightarrow C \cdot S + 4S \qquad \text{(Phenol hydrogenation)} \qquad \text{(S17)}$$

$$C \cdot S + 2H \cdot S \leftrightarrow D \cdot S + 2S \qquad \text{(Cyclohexanone hydrogenation)} \qquad \text{(S18)}$$

Route 2: Ring Saturation – Demethoxylation

$$A \cdot S + 4H \cdot S \leftrightarrow E \cdot S + 4S \qquad \text{(Guaiacol hydrogenation)} \qquad \text{(S19)}$$

$$E \cdot S + 2H \cdot S \leftrightarrow F \cdot S + 2S \qquad \text{(2-Methoxycyclohexanone hydrogenation)} \qquad \text{(S20)}$$

$$F \cdot S + 2H \cdot S \leftrightarrow D \cdot S + G \cdot S + S \qquad \text{(2-Methoxycyclohexanol hydrogenation)} \qquad \text{(S21)}$$
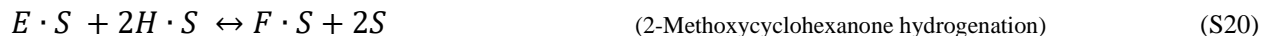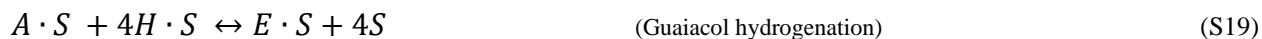
Note that the sum of all elementary steps in Route 1 or 2 generates the overall reaction as follows:

$$A \cdot S + 8H \cdot S \leftrightarrow D \cdot S + G \cdot S + 7S \qquad \text{(Overall surface reaction)} \qquad \text{(S22)}$$
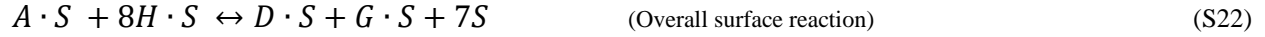
The ECH of guaiacol taking place in the catalyst consists of consecutive reactions in the parallel pathways rather than a single-step reaction. In such complex chemical reaction, the relative reaction rate of the intermediate products can become dependent on diffusive conditions [9]. In this study, the model is simplified by focusing on the overall guaiacol ECH as the reference point for the surface reaction.

Product desorption steps can be written as follows:

$$B \cdot S \leftrightarrow B + S \qquad \text{(Phenol desorption)} \qquad \text{(S23)}$$

$$C \cdot S \leftrightarrow C + S \qquad \text{(Cyclohexanone desorption)} \qquad \text{(S24)}$$
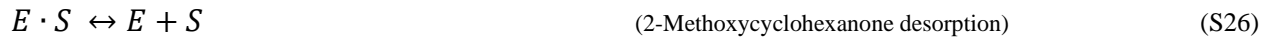
$$D \cdot S \leftrightarrow D + S \qquad \text{(Cyclohexanol desorption)} \qquad \text{(S25)}$$

$$E \cdot S \leftrightarrow E + S \qquad \text{(2-Methoxycyclohexanone desorption)} \qquad \text{(S26)}$$

$$F \cdot S \leftrightarrow F + S \qquad \text{(2-Methoxycyclohexanol desorption)} \qquad \text{(S27)}$$

$$G \cdot S \leftrightarrow G + S \qquad \text{(Methanol desorption)} \qquad \text{(S28)}$$
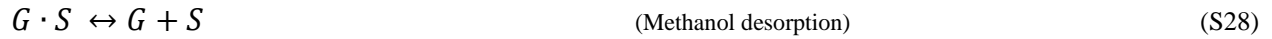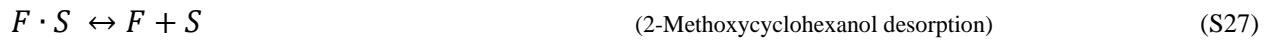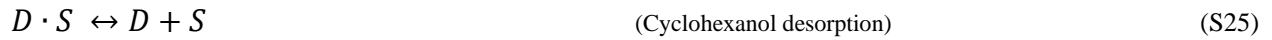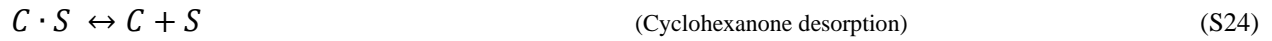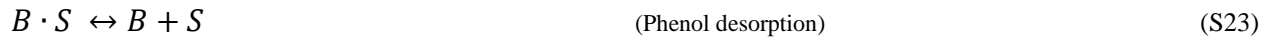
Possible scenarios for the RDS are derived step-by-step to propose the rate law that best fits the experimental data:

Case 1: Adsorption of guaiacol is the RDS

The rate expression is derived from Equation S14:

$$r_a = k_a C_A C_v - k_{-a} C_{A \cdot S} = k_a \left(C_A C_v - \frac{C_{A \cdot S}}{K_a} \right) \qquad \text{(S29)}$$

Note: $K_a = k_a / k_{-a}$ is the adsorption equilibrium constant, C_v is the concentration of vacant sites.

Analogously, the rate expressions for the other elementary steps (Equations S15, S22, S25, S28) can be derived as follows:

$$r_H = k_H C_H C_v - k_{-H} C_{H \cdot S} = k_H \left(C_H C_v - \frac{C_{H \cdot S}}{K_H} \right) \tag{S30}$$

$$r_s = k_s C_{A \cdot S} C_{H \cdot S}^8 - k_{-s} C_{D \cdot S} C_{G \cdot S} C_v^7 = k_s \left(C_{A \cdot S} C_{H \cdot S}^8 - \frac{C_{D \cdot S} C_{G \cdot S} C_v^7}{K_s} \right) \tag{S31}$$

Note that the overall surface reaction is used to formulate the rate expression: the power of 8 ($C_{H \cdot S}$) refers to the number of protons/electrons involved while the power of 7 (C_v) refers to the number of compounds involved in the overall guaiacol ECH reaction.

For simplification purposes, the rate expressions for desorption steps exclusively take into account the overall products (cyclohexanol and methanol):

$$r_{d,D} = k_{d,D} C_{D \cdot S} - k_{-d,D} C_{D \cdot S} C_v = k_{d,D} \left(C_{D \cdot S} - K_{d,D} C_D C_v \right) \tag{S32}$$

$$r_{d,G} = k_{d,G} C_{G \cdot S} - k_{-d,G} C_{G \cdot S} C_v = k_{d,G} \left(C_{G \cdot S} - K_{d,G} C_G C_v \right) \tag{S33}$$

Since the guaiacol adsorption is the RDS, proton chemisorption, surface reaction, and product desorption proceed fast, giving large k_H, k_s, and k_d by comparison, thus r_H/k_H, r_s/k_s, and r_d/k_d in Equations S30–S33 will be approximate to zero.

The equilibrium concentrations of adsorbed reactants and products can then be obtained as follows:

$$C_{H \cdot S} = K_H C_H C_v \tag{S34}$$

$$C_{A \cdot S} = \frac{C_{D \cdot S} C_{G \cdot S} C_v^7}{K_s C_{H \cdot S}^8} \tag{S35}$$

$$C_{D \cdot S} = K_{d,D} C_D C_v \tag{S36}$$

$$C_{G \cdot S} = K_{d,G} C_G C_v \tag{S37}$$

Equations S34–S37 can be combined and rearranged to obtain $C_{A \cdot S}$:

$$C_{A \cdot S} = \frac{K_{d,D} C_D K_{d,G} C_G C_v}{K_S (K_H C_H)^8} \tag{S38}$$

Site balance: $C_t = C_v + C_{A \cdot S} + C_{H \cdot S} + C_{D \cdot S} + C_{G \cdot S}$ (S39)

Equations S34, S36–S38 can be substituted into Equation S39 to obtain C_v:

$$C_v = C_t \Big/ \left(1 + \frac{K_{d,D} C_D K_{d,G} C_G}{K_S (K_H C_H)^8} + K_H C_H + K_{d,D} C_D + K_{d,G} C_G \right) \tag{S40}$$

Finally, Equations S38 and S40 are substituted into Equation S29 to obtain the rate expression for guaiacol adsorption:

$$r_a = \frac{C_t k_a \left(C_A - \frac{K_{d,D} C_D K_{d,G} C_G}{K_a K_S (K_H C_H)^8} \right)}{\left(1 + \frac{K_{d,D} C_D K_{d,G} C_G}{K_S (K_H C_H)^8} + K_H C_H + K_{d,D} C_D + K_{d,G} C_G \right)} \tag{S41}$$

The initial rate of reaction (r_{a0}) as a function of guaiacol concentration (C_{A0}) is now given by:

$$\boxed{r_{a0} = \frac{C_t k_a C_{A0}}{1 + K_H C_H} = k C_{A0}} \tag{S42}$$

(Initially, no products are present, thus $C_{D0} = C_{G0} = 0$)

Assuming the proton concentration is constantly abundant (as continuously supplied from the water splitting reactions), $r_{a,0}$ becomes linearly dependent on C_{A0} and can be written as:

$r_{a0} = k C_{A0}$ (where $k = \frac{C_t k_a}{1 + K_H C_H}$).

Case 2: Surface reaction is the RDS

The rate expression is derived from Equation S31:

$$r_s = k_s \left(C_{A \cdot S} C_{H \cdot S}^8 - \frac{C_{D \cdot S} C_{G \cdot S} C_v^7}{K_S} \right) \tag{S31}$$

In the similar manner as in Case 1 (to derive Equations S34–S37), $C_{A\cdot S}$, $C_{H\cdot S}$, $C_{D\cdot S}$, and $C_{G\cdot S}$ can be obtained to solve for Equation S31, in combination with C_v expression from the site balance:

$$C_{A\cdot S} = K_a C_A C_v \tag{S43}$$

$$C_v = C_t / \left(1 + K_a C_A + K_H C_H + K_{d,D} C_D + K_{d,G} C_G\right) \tag{S44}$$

Thus, the rate expression for surface reaction can be written as follows:

$$r_S = \frac{C_t^9 k_S \left(K_a C_A (K_H C_H)^8 - \frac{K_{d,D} C_D K_{d,G} C_G}{K_S}\right)}{\left(1 + K_a C_A + K_H C_H + K_{d,D} C_D + K_{d,G} C_G\right)} \tag{S45}$$

The initial rate of reaction (r_{s0}) is obtained when $C_{D0} = C_{G0} = 0$:

$$\boxed{r_{s0} = \frac{C_t^9 k_S \left(K_a C_{A0} (K_H C_H)^8\right)}{1 + K_a C_{A0} + K_H C_H} = \frac{k(C_{A0})}{1 + K_a C_{A0} + K_H C_H}} \qquad \{\text{where } k = C_t^9 k_S (K_H C_H)^8 K_a\} \tag{S46}$$

This expression implies two possible consequences if the RDS is the surface reaction:

- At low concentrations of A: $(1 + K_H C_H \gg K_a C_{A0})$, hence: $r_{s0} = \frac{k(C_{A0})}{1 + K_H C_H} = k' C_{A0}$

  → The initial reaction rate is linearly dependent on guaiacol concentration.

- At high concentrations of A: $(K_a C_{A0} \gg 1 + K_H C_H)$, hence: $r_{s0} = \frac{k(C_{A0})}{K_a C_{A0}} = k''$

  → The initial reaction rate is independent of guaiacol concentration.

Case 3: Desorption of the product is the RDS

The rate expression derivation starts with Equation S32 or S33 with two possible scenarios:

a. If cyclohexanol desorption is limiting: $\qquad r_{d,D} = k_{d,D}\left(C_{D\cdot S} - K_{d,D} C_D C_v\right) \tag{S32}$

b. If methanol desorption is limiting: $\qquad r_{d,G} = k_{d,G}\left(C_{G\cdot S} - K_{d,G} C_G C_v\right) \tag{S33}$

In order to solve for $C_{D\cdot S}$ and $C_{G\cdot S}$, $C_{A\cdot S}$ is first determined when $r_s/k_s \approx 0$ (see Equation S38) and then rearranged to obtain:

$$C_{D \cdot S} = \frac{K_a C_A K_S (K_H C_H)^8 C_v}{K_{d,G} C_G} \tag{S47}$$

$$C_{G \cdot S} = \frac{K_a C_A K_S (K_H C_H)^8 C_v}{K_{d,D} C_D} \tag{S48}$$

From the site balance, C_v can be obtained for each case above:

For Case (a): $C_v = C_t \Big/ \left(1 + K_a C_A + K_H C_H + \frac{K_a C_A K_S (K_H C_H)^8}{K_{d,G} C_G} + K_{d,G} C_G \right)$ (S49)

For Case (b): $C_v = C_t \Big/ \left(1 + K_a C_A + K_H C_H + K_{d,D} C_D + \frac{K_a C_A K_S (K_H C_H)^8}{K_{d,D} C_D} \right)$ (S50)

Finally, Equations S47 and S49 are substituted into Equation S32 (in the same manner, Equations S48 and S50 into Equation S33) to obtain the rate expressions for desorption control as follows:

$$r_{d,D} = \frac{C_t k_{d,D} \left(\frac{K_a C_A K_S (K_H C_H)^8}{K_{d,G} C_G} - K_{d,D} C_D \right)}{1 + K_a C_A + K_H C_H + \frac{K_a C_A K_S (K_H C_H)^8}{K_{d,G} C_G} + K_{d,G} C_G} = \frac{C_t k_{d,D} \left(\frac{K_a C_A K_S (K_H C_H)^8}{K_{d,G}} - K_{d,D} C_D C_G \right)}{C_G + K_a C_A C_G + K_H C_H C_G + \frac{K_a C_A K_S (K_H C_H)^8}{K_{d,G}} + K_{d,G} C_G^2} \tag{S51}$$

$$r_{d,G} = \frac{C_t k_{d,G} \left(\frac{K_a C_A K_S (K_H C_H)^8}{K_{d,D} C_D} - K_{d,G} C_G \right)}{1 + K_a C_A + K_H C_H + K_{d,D} C_D + \frac{K_a C_A K_S (K_H C_H)^8}{K_{d,D} C_D}} = \frac{C_t k_{d,G} \left(\frac{K_a C_A K_S (K_H C_H)^8}{K_{d,D}} - K_{d,G} C_G C_D \right)}{C_D + K_a C_A C_D + K_H C_H C_D + K_{d,D} C_D^2 + \frac{K_a C_A K_S (K_H C_H)^8}{K_{d,D}}} \tag{S52}$$

The initial rate of reaction (r_{d0}) is obtained when $C_{D0} = C_{G0} = 0$, thereby simplifying the above equations into:

$$\boxed{r_{d,D0} = \frac{C_t k_{d,D} \left(\frac{K_a C_{A0} K_S (K_H C_H)^8}{K_{d,G}} \right)}{\frac{K_a C_{A0} K_S (K_H C_H)^8}{K_{d,G}}} = C_t k_{d,D}} \tag{S53}$$

$$\boxed{r_{d,G0} = \frac{C_t k_{d,G} \left(\frac{K_a C_{A0} K_S (K_H C_H)^8}{K_{d,D}} \right)}{\frac{K_a C_{A0} K_S (K_H C_H)^8}{K_{d,D}}} = C_t k_{d,G}} \tag{S54}$$

The bracketed terms on numerator and the denominator terms are cancelled out. Thus, if desorption were the RDS, the initial reaction rate would be constant for different concentration values (i.e. independent of the initial guaiacol concentration, and the relationship between r_{d0} and C_{A0} would be plotted as a flat line with zero gradient).

In summary, the following trends will be observed if the RDS is:

- Adsorption: the initial reaction rate is linearly dependent on guaiacol concentration.

- Surface reaction: the initial reaction rate is linearly dependent on guaiacol concentration (at low concentrations) but independent of guaiacol concentration (at high concentrations).

- Desorption: the initial reaction rate would be independent of guaiacol concentration.

Verifying the reaction mechanism with experimental data

Guaiacol ECH experiments were carried out in acidic electrolytes (H_2SO_4 and MSA with the same concentration) under potentiostatic and galvanostatic conditions, respectively (Figure S3). Similar trends were observed in terms of initial reaction rate ($-r_{A0}$) and Faradaic efficiency (F.E.), which increased with the guaiacol concentration. The higher guaiacol concentration promotes F.E. as the surface coverage of organic molecules increased. Consequently, at nearly complete guaiacol conversion (>99%), H_2 evolution reaction became more dominant, thus lowering the F.E. Under potentiostatic control, cyclohexanol (~52%) and 2-methoxycyclohexanol (27–35%) were the most selective products (Figure S3a). However, under temperature-controlled galvanostatic conditions ($T = 50$ °C), demethoxylation of guaiacol was favored over ring saturation by the increasing temperature, resulting in the higher cyclohexanone (18–28%) and the lower 2-methoxycyclohexanol (9–18%) selectivities (Figure S3b). In both cases, a linear relationship is obtained between the initial reaction rate and the guaiacol concentration (50–130 mM) under the

applied conditions (Figures S4c–d). These results demonstrate that the ECH of guaiacol in this work is either adsorption-limited or surface reaction-limited (at low concentrations), consistent with the rate law formulation described earlier. The limitations of this kinetic model approach include inability to distinguish: (i) the amount of H_{ads} coverage for ECH and HER, (ii) the active sites for organic reactant adsorption and proton reduction, and (iii) the amount of surface sites for each different pathway in the guaiacol ECH.
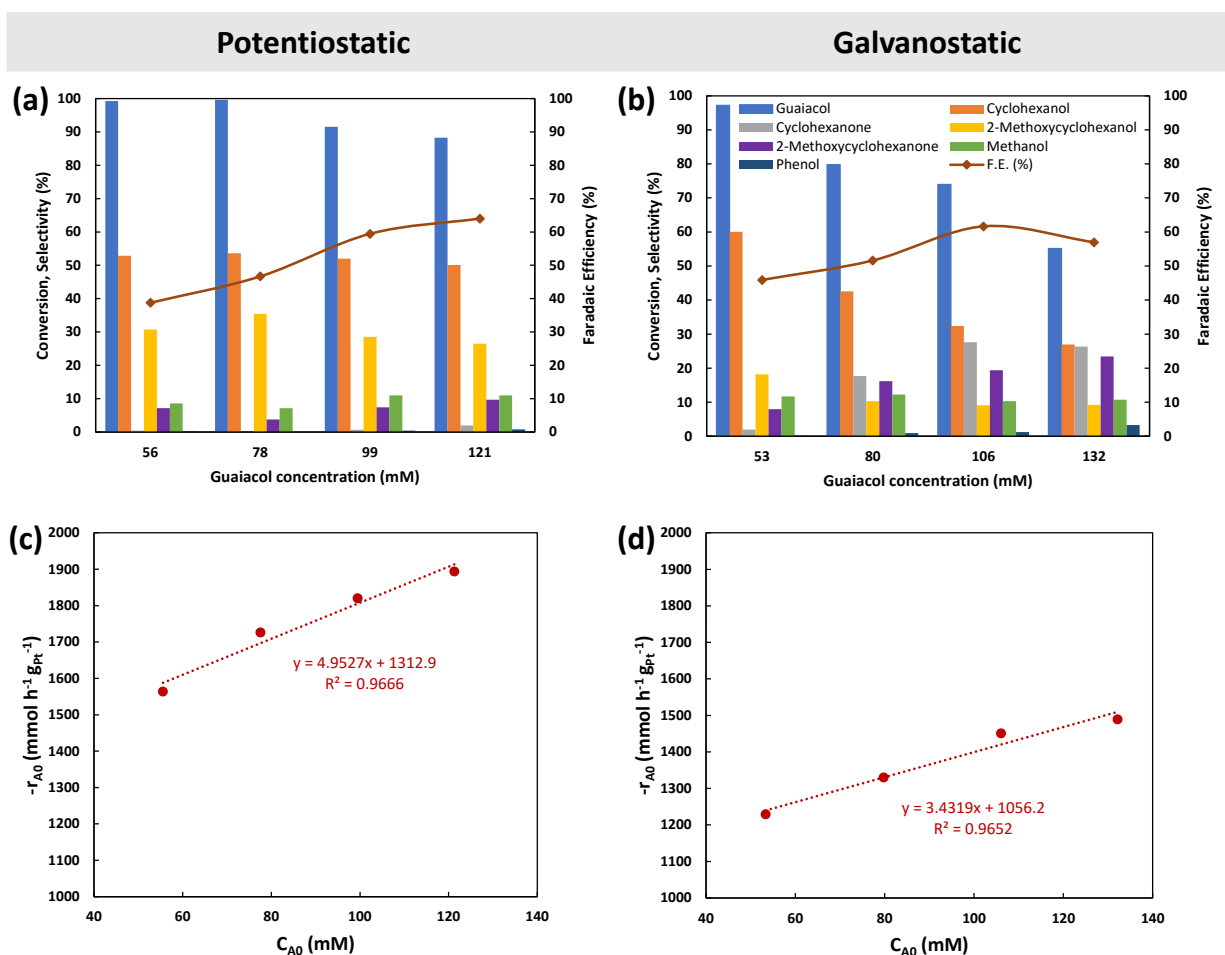
Figure S3. ECH of guaiacol under potentiostatic (a) and galvanostatic (b) conditions in H_2SO_4 (0.2 M) and MSA (0.2 M) electrolytes, respectively. Upper panel (a–b): Guaiacol conversion, product selectivity, and Faradaic efficiency profiles at different initial guaiacol concentrations. Lower panel (c–d): Initial reaction rate as a function of initial guaiacol concentration showing a linear relationship, thus implying that adsorption is the RDS under the operating conditions. Experimental conditions: (a, c) E = -1.25 V (vs. Ag/AgCl), $j \approx$ -182 to -218 mA cm⁻², $T \approx$ 40 °C, t = 4 h, Catalyst: 5 wt.%-Pt/C (0.10 g); (b, d) j = -182 mA cm⁻², $E \approx$ -1.09 V to -1.29 V (vs. Ag/AgCl), T = 50 °C, t = 4 h, Catalyst: 5 wt.%-Pt/C (0.15 g). Initial reaction rates were measured after 1 h.

Galvanostatic guaiacol ECH results

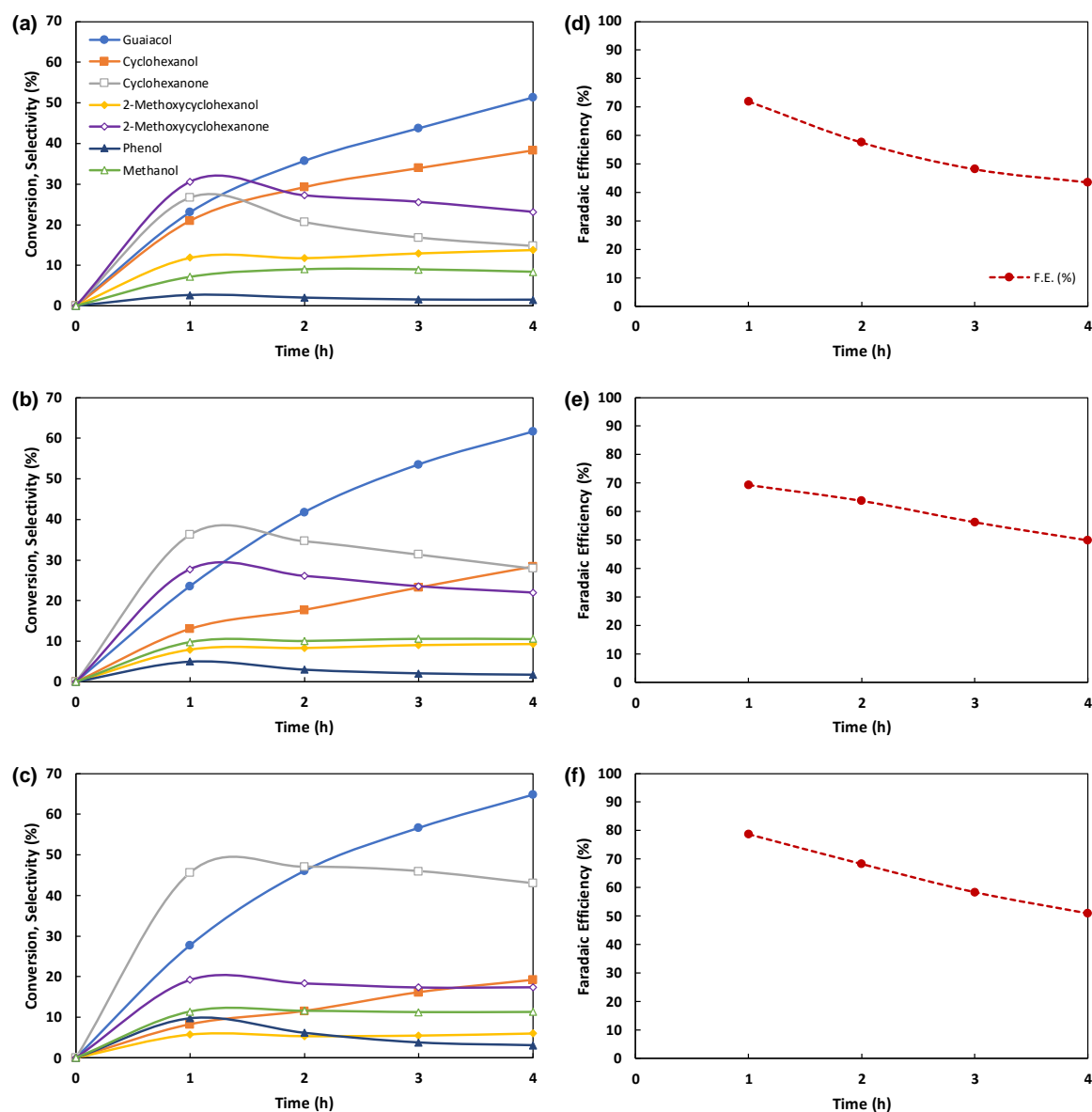## Temperature effect with different catalyst loadings and stirring profiles in the SSER

Figure S4. ECH of guaiacol in MSA electrolyte (0.2 M). Guaiacol conversion and product selectivity profiles at different temperatures: (a) 40 °C (b) 50 °C, (c) 60 °C. Faradaic efficiency profiles for the corresponding results (d, e, f). Reaction conditions: I = -0.5 A (j = -182 mA cm^{-2}), t = 4 h, R_d = 240 rpm (Stirrer B). Catalyst: 5 wt%-Pt/C (0.10 g, corresponding to loading in SSER of 7 wt.%), R/M ≈ 419. Guaiacol concentration (initial) = 106 mM. Catholyte pH ≈ 0.8–0.9. The apparent reaction order = 2 (vs. guaiacol).
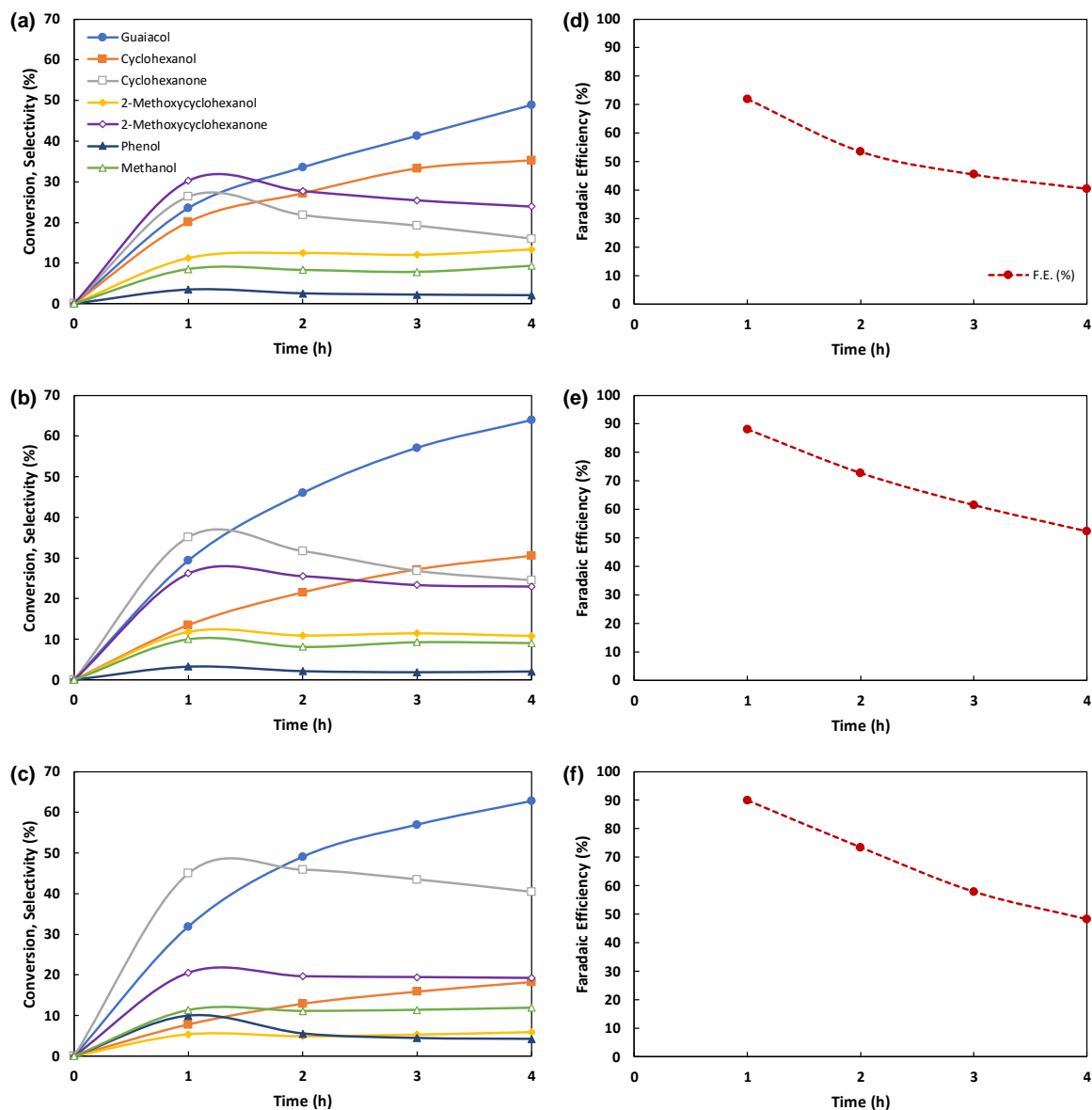
Figure S5. ECH of guaiacol in MSA electrolyte (0.2 M). Guaiacol conversion and product selectivity profiles at different temperatures: (a) 40 °C (b) 50 °C, (c) 60 °C. Faradaic efficiency profiles for the corresponding results (d, e, f). Reaction conditions: I = -0.5 A (j = -182 mA cm^{-2}), t = 4 h, R_d = 500 rpm (Stirrer A). Catalyst: 5 wt%-Pt/C (0.15 g, corresponding to concentration of 10 wt.%), R/M ≈ 279. Guaiacol concentration (initial) = 106 mM. Catholyte pH ≈ 0.8–0.9. The apparent reaction order = 2 (vs. guaiacol).
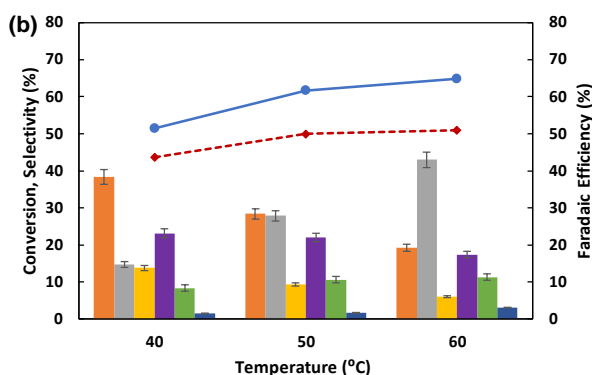
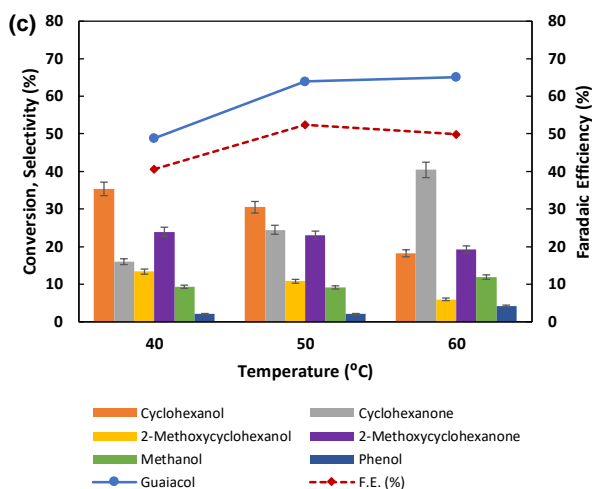**(a)**
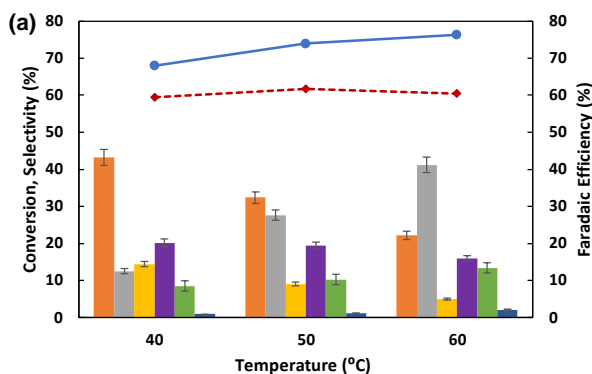
T (°C)	E$_{cathode}$ (V)
40	-1.193
50	-1.090
60	-1.001

(b)

T (°C)	E$_{cathode}$ (V)
40	-1.234
50	-1.093
60	-0.931

(c)

T (°C)	E$_{cathode}$ (V)
40	-1.322
50	-1.267
60	-1.210

Legend: Cyclohexanol, Cyclohexanone, 2-Methoxycyclohexanol, 2-Methoxycyclohexanone, Methanol, Phenol, Guaiacol, F.E. (%)

Figure S6. Guaiacol conversion, product selectivity, and Faradaic efficiency at different temperatures and I = -0.5 A (j = -182 mA cm^{-2}) after 4 h. Catalyst (5 wt%-Pt/C) with different loading (concentration): (a) 0.15 g (10 wt.%), (b) 0.10 g (7 wt.%), (c) 0.15 g (10 wt.%). Stirring rate (R$_d$) and stirrer size (L): (a) 240 rpm, 3.6 cm, (b) 240 rpm, 3.6 cm, (c) 500 rpm, 2.4 cm. Guaiacol concentration (initial) = 106 mM. $E_{cathode}$ = average cathode potential during the electrolysis. In all cases, the increasing temperature resulted in the lower cathode potential (vs. Ag/AgCl) and thus affecting the product distribution. This potential-temperature synergistic effect has also been observed in the previous work using H$_2$SO$_4$ electrolyte.[1]

Kinetic analysis for guaiacol ECH reaction order and the rate constant estimations

Basic approach: $A\,(Guaiacol) \rightarrow B$, the rate of reaction: $\frac{dC_A}{dt} = -kC_A^{\alpha}$
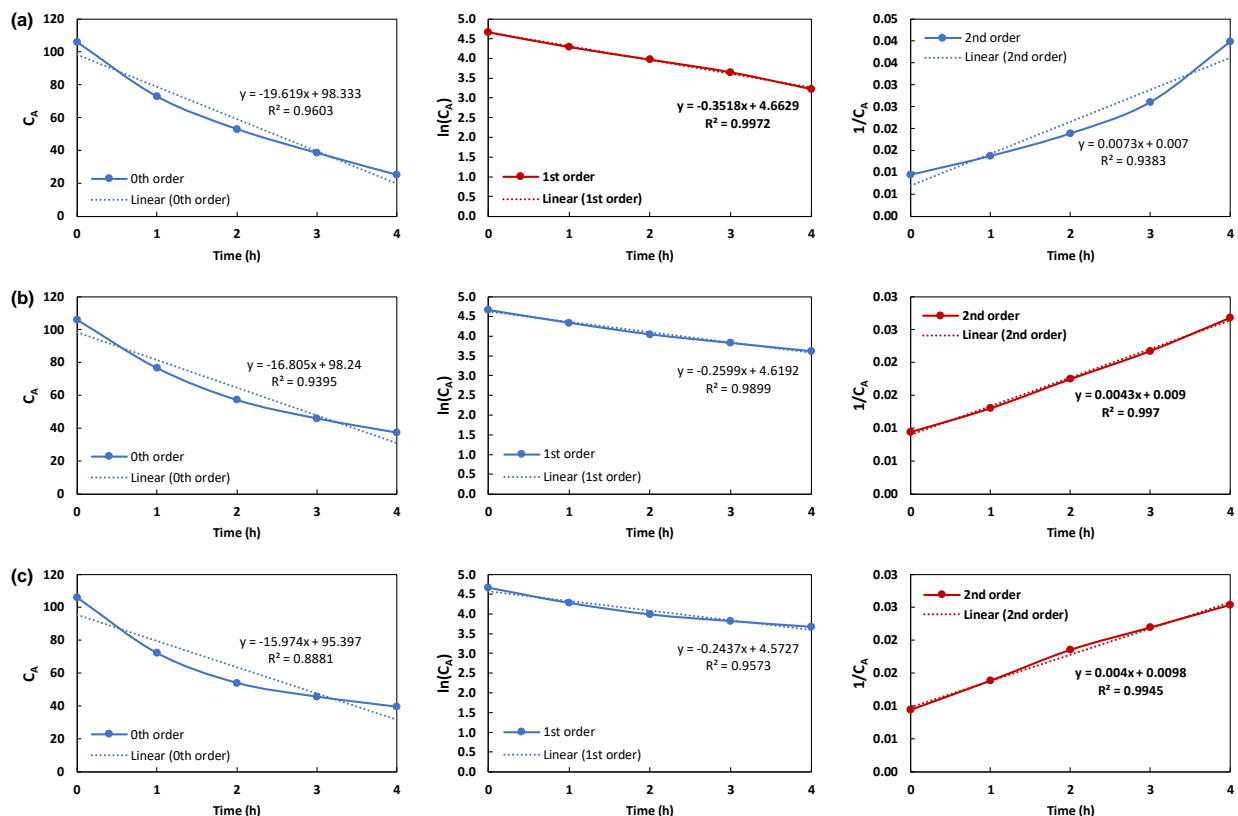
Condition	Reaction order	Rate constant expression	Rate constant (k) values			Unit
			40 °C	50 °C	60 °C	
(a)	1st	$lnC_A = lnC_{A0} - kt$ $k = \frac{ln(C_{A0}/C_A)}{t}$	8.0×10^{-5} (7.20)	9.0×10^{-5} (8.09)	1.0×10^{-4} (8.98)	s^{-1} (s^{-1} mol_{Pt}^{-1})
(b)	2nd	$1/C_A = 1/C_{A0} + kt$ $k = \frac{1/C_A - 1/C_{A0}}{t}$	7.2×10^{-4} (97.3)	9.5×10^{-4} (128.3)	1.1×10^{-3} (150.6)	M^{-1} s^{-1} (M^{-1} s^{-1} mol_{Pt}^{-1})
(c)	2nd	$1/C_A = 1/C_{A0} + kt$ $k = \frac{1/C_A - 1/C_{A0}}{t}$	6.8×10^{-4} (60.7)	1.1×10^{-3} (101.7)	1.2×10^{-3} (106.8)	M^{-1} s^{-1} (M^{-1} s^{-1} mol_{Pt}^{-1})

Figure S7. Graphical analysis for the apparent reaction order and rate constant determination in ECH of guaiacol using MSA (0.2 M) electrolyte pairs with different catalyst loading in the SSERs, stirring rates, and stirrer sizes: (a) 10 wt.%, 240 rpm, 3.6 cm [Figures 2, S7a], (b) 7 wt.%, 240 rpm, 3.6 cm [Figures S5, S7b], (c) 10 wt.%, 500 rpm, 2.4 cm [Figures S6, S7c]. Reaction conditions in Figures (a–c): I = -0.5 A (j = -182 mA cm^{-2}), T = 60 °C, t = 4 h. The table shows the rate constant for each temperature under the different conditions with the values in brackets are determined by normalization with the catalyst active sites (dispersed Pt molar amount).

Complementary results and data

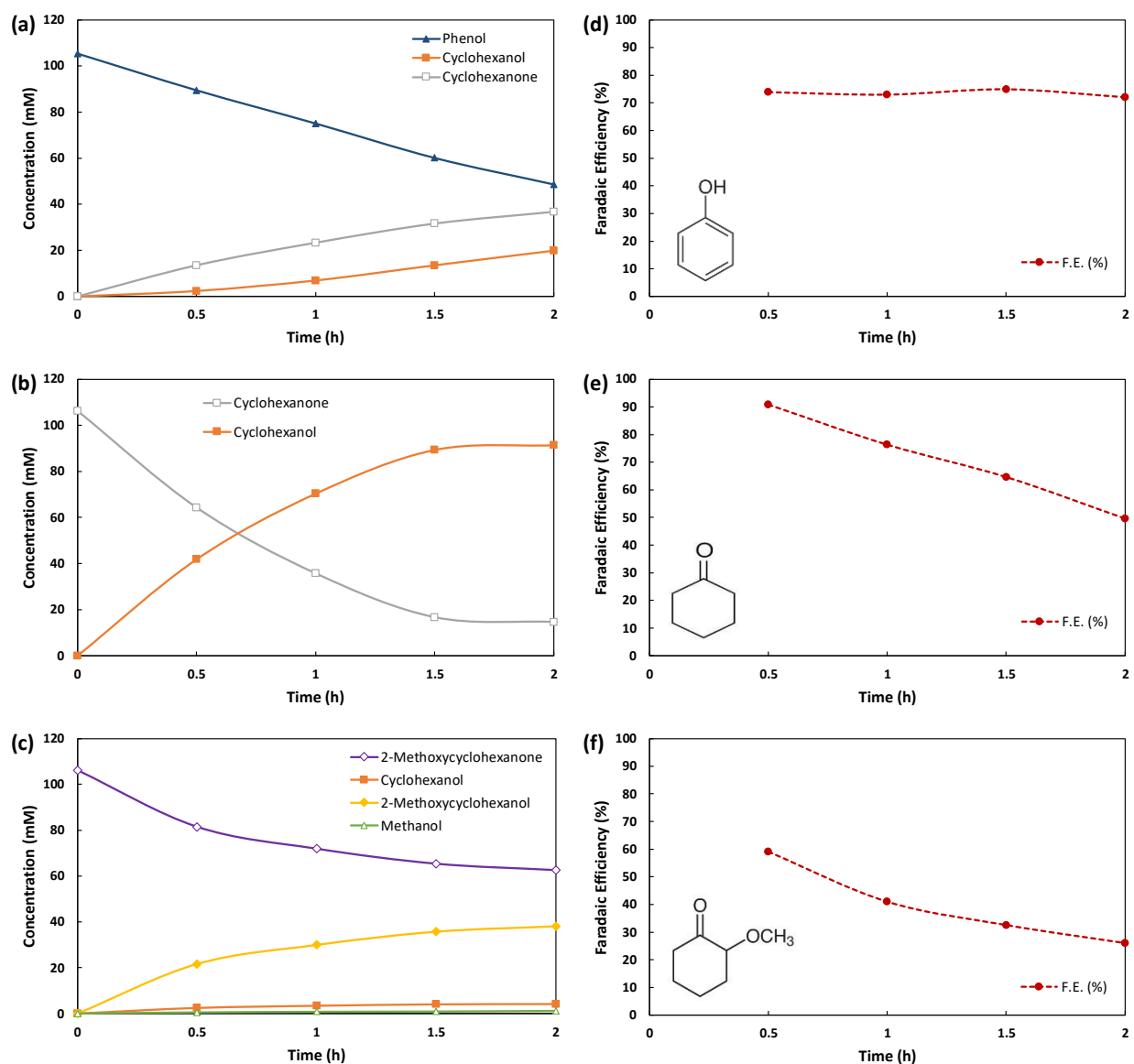## ECH of intermediate reactants for reaction order determination

Figure S8. Concentration and Faradaic efficiency profiles from ECH of intermediate reactant: (a, d) phenol, (b, e) cyclohexanone, (c, f) 2-methoxycyclohexanone. Reaction conditions: $I = -0.5$ A ($j = -182$ mA cm^{-2}), $T = 50$ °C, $t = 2$ h, $R_d = 240$ rpm (Stirrer B). Catalyst: 5 wt%-Pt/C (0.15 g, corresponding to concentration of 10 wt.%). Initial reactant concentration = 0.1 M. Catholyte pH ≈ 0.8. The apparent reaction order: (a) 0th or 1st (vs. phenol), (b) 1st (vs. cyclohexanone), (c) 2nd (vs. 2-methoxycyclohexanone).

MATLAB codes for the ECH of guaiacol kinetics

```matlab
% kinfit.m
% This program evaluates the parameter estimation method to determine rate
% constants of each reaction in the ECH of guaiacol pathways.
% This program uses Levenberg-Marquardt method for the nonlinear regression of
% the model and actual data from the ECH experiments.

clear all
clc
clf

% Initialization and input specification
Data = readtable('ch-data60.xlsx'); % Experimental concentration data

% Declare the variables to all the functions
global CA0 CB0 CC0 CD0 CE0 CF0 Cex C tspan sse SD
CA0 = 106.03; CB0 = 0; CC0 = 0; CD0 = 0; CE0 = 0; CF0 = 0;
Cex = table2array(Data(:,2:7)); % Convert table to homogeneous array
tspan = table2array(Data(:,1));
k0 = [0.01 0.01 0.01 0.01 0.01 0.01]; % Initial values in a row vector
lb = zeros (1,6); % Lower bounds
ub = 1000*ones(1,6); % Upper bounds

% Optimization options structure using 'lsqnonlin' to solve nonlinear
% least-squares (nonlinear data-fitting) problems and the default algorithm
% is a so-called 'trust-region reflective' that requires the number of
% equations (i.e. the row dimension of F) to be at least as great as the
% number of variables. The alternative algorithm is 'levenberg-marquardt'
% which uses unbound constraints.
options = optimoptions(@lsqnonlin,'Display','Iter');
[k,resnorm,res, exitflag,output,lambda,J]=lsqnonlin(@optim,k0,lb,ub,options)

% nonlinear regression parameter confidence intervals to compute 95%
% confidence intervals
Ci = nlparci(k,res,'Jacobian',J)
Cex; % Measured dependent variables
C; % Calculated dependent variables
t=tspan'; % Independent variables

% Plot of guaiacol concentration (real vs. model)
figure(1)
plot(t,C(:,1),'b-');
xlabel('Time (h)');
ylabel('Concentration (mM)');
xticks([0:0.5:4]);
hold on;
plot(t,Cex(:,1),'ob');
legend({'A model','A real'});
hold off
```

```matlab
% Plot of product concentration (real vs. model)
figure(2)
plot(t,C(:,2),'r--',t,C(:,3),'k-.',t,C(:,4),'k--',t,C(:,5),'m-.',t,C(:,6),'k:');
xlabel('Time (h)');
xticks([0:0.5:4]);
ylabel('Concentration (mM)');
hold on;
plot(t,Cex(:,2),'dr',t,Cex(:,3),'ok',t,Cex(:,4),'sk',t,Cex(:,5),'*m',t,Cex(:,6),'^k');
legend({'B model','C model','D model','E model','F model','B real','C real','D real','E real','F real'});
hold off;

% Output declaration
sse
SD
k

% Integrate the ODEs using Runge-Kutta 4 method
function [sse, SD] =optim(k);
global CA0 CB0 CC0 CD0 CE0 CF0 Cex C tspan sse SD
[t,C] = ode45(@balance,tspan,[CA0 CB0 CC0 CD0 CE0 CF0]);

% Function to be integrated
function dCdt=balance(t,C)
dCdt=zeros(6,1); % Initialization

% Material balance expression
CT=C(1)+C(2)+C(3)+C(4)+C(5)+C(6);
CA = CA0*(C(1)/CT);
CB = CA0*(C(2)/CT);
CC = CA0*(C(3)/CT);
CD = CA0*(C(4)/CT);
CE = CA0*(C(5)/CT);
CF = CA0*(C(6)/CT);

% ODEs model: multiple equations, multiple parameters
dCdt(1) = -k(1)*CA-k(4)*CA;
dCdt(2) = k(1)*CA-k(2)*CB;
dCdt(3) = k(2)*CB-k(3)*CC;
dCdt(4) = k(3)*CC+k(6)*CF^2;
dCdt(5) = k(4)*CA-k(5)*CE^2;
dCdt(6) = k(5)*CE^2-k(6)*CF^2;

end

nt=length(tspan);
Cmod = C;
sse = (Cmod-Cex).^2; % sum of squares of the residual
SD = sqrt(sum(sse)/nt); % standard deviation
end
```

Standard deviation between model and actual data:

$$SD = \sqrt{\frac{1}{N}\sum_{i=1}^{N}|C_{i,a} - C_{i,m}|^2}$$

	40 ºC	50 ºC	60 ºC
A	2.76	1.65	1.79
B	1.12	1.32	1.52
C	1.59	1.55	1.84
D	1.95	1.36	1.46
E	1.67	1.61	1.72
F	2.11	1.52	1.28

Note: SD = standard deviation, N = number of data, $C_{i,a}$ = actual concentration data, $C_{i,m}$ = model concentration data.

Compound label: A = guaiacol, B = phenol, C = cyclohexanone, D = cyclohexanol, E = 2-methoxycyclohexanone, F = 2-methoxycyclohexanol.

Polarization tests with MSA electrolyte
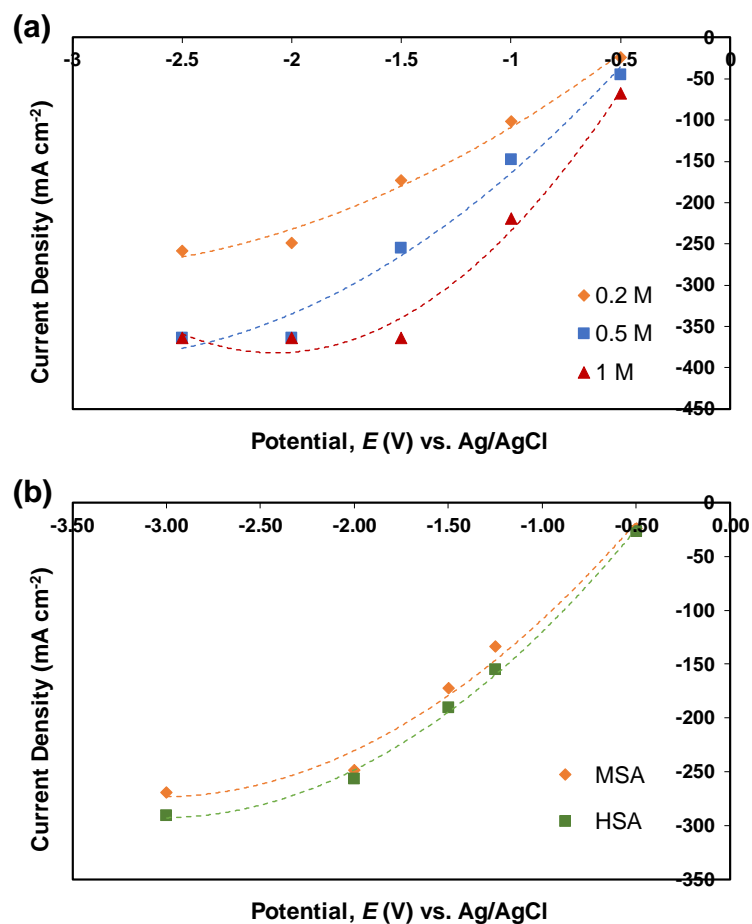
(a)

(b)

Figure S9. Polarization curves using (a) MSA electrolyte with different concentrations (0.2 M, 0.5 M, 1 M), (b) MSA electrolyte in comparison to sulfuric acid (HSA) electrolyte with the same concentration (0.2 M). Cathode geometrical size: 2.5 cm × 1.1 cm.

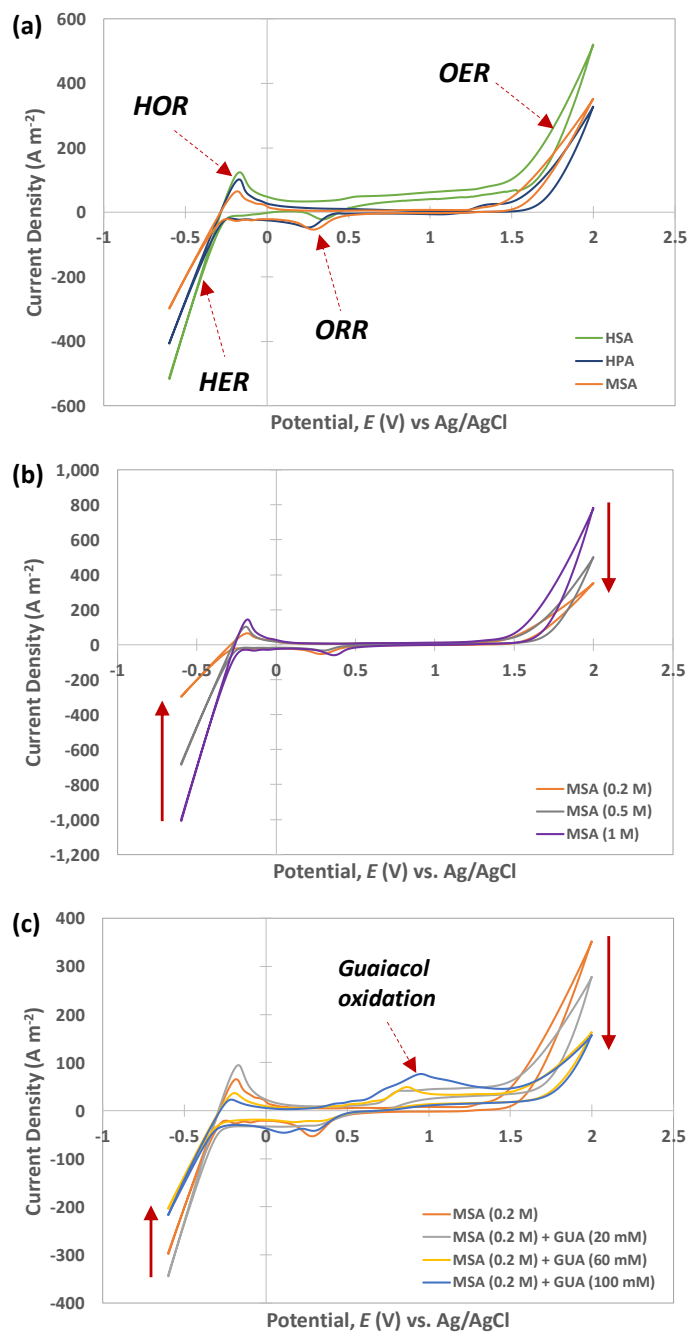# Cyclic voltammetry with different acid electrolytes

Figure S10. Cyclic voltammograms on Pt gauze using different electrolytes: (a) sulfuric acid (HSA), perchloric acid (HPA), and methanesulfonic acid (MSA) electrolytes (concentration: 0.2 M); (b) MSA with different concentrations; (c) MSA with different guaiacol concentrations. Hydrogen evolution (HER), hydrogen oxidation (HOR), oxygen evolution (OER), and oxygen reduction (ORR) reactions are identified in all cases.

References

(1)   Wijaya, Y. P.; Grossmann-Neuhaeusler, T.; Dhewangga Putra, R. D.; Smith, K. J.; Kim, C. S.; Gyenge, E. L. Electrocatalytic Hydrogenation of Guaiacol in Diverse Electrolytes Using a Stirred Slurry Reactor. *ChemSusChem* **2020**, *13* (3), 629–639, DOI 10.1002/cssc.201902611.

(2)   Wijaya, Y. P.; Smith, K. J.; Kim, C. S.; Gyenge, E. L. Synergistic Effects between Electrocatalyst and Electrolyte in the Electrocatalytic Reduction of Lignin Model Compounds in a Stirred Slurry Reactor. *J. Appl. Electrochem.* **2020**, *51*, 51–63, DOI 10.1007/s10800-020-01429-w.

(3)   Mears, D. E. Tests for Transport Limitations in Experimental Catalytic Reactors. *Ind. Eng. Chem. Process Des. Dev.* **1971**, *10* (4), 541–547, DOI 10.1021/i260040a020.

(4)   Masende, Z. P. G.; Kuster, B. F. M.; Ptasinski, K. J.; Janssen, F. J. J. G.; Katima, J. H. Y.; Schouten, J. C. Platinum Catalysed Wet Oxidation of Phenol in a Stirred Slurry Reactor: A Practical Operation Window. *Appl. Catal. B Environ.* **2003**, *41* (3), 247–267, DOI 10.1016/S0926-3373(02)00164-9.

(5)   Yadav, G. D.; Pathre, G. S. Selectivity Engineering of Cation-Exchange Resins over Inorganic Solid Acids in C-Alkylation of Guaiacol with Cyclohexene. *Ind. Eng. Chem. Res.* **2007**, *46* (10), 3119–3127, DOI 10.1021/ie060645t.

(6)   Kumbhar, P. S.; Yadav, G. D. Catalysis by Sulfur-Promoted Superacidic Zirconia: Condensation Reactions of Hydroquinone with Aniline and Substituted Anilines. *Chem. Eng. Sci.* **1989**, *44* (2), 2535–2544, DOI 10.1016/0009-2509(89)85197-8.

(7)   Fogler, H. S. *Essentials of Chemical Reaction Engineering, 2nd Edition*; Pearson Prentice Hall, **2017**.

(8)   Song, Y.; Gutiérrez, O. Y.; Herranz, J.; Lercher, J. A. Aqueous Phase Electrocatalysis and Thermal Catalysis for the Hydrogenation of Phenol at Mild Conditions. *Appl. Catal. B Environ.* **2016**, *182*, 236–246, DOI 10.1016/j.apcatb.2015.09.027.

(9)   Weisz, P. B.; Prater, C. D. Interpretation of Measurements in Experimental Catalysis. *Adv. Catal.* **1954**, *6* (C), 143–196, DOI 10.1016/S0360-0564(08)60390-9.